# Three-Dimensional Unsteady Wake Characteristics of Rectangular Cylinder

IOP Conf. Series: Journal of Physics: Conf. Series **1240** (2019) 012060 doi:10.1088/1742-6596/1240/1/012060

# Three-Dimensional Unsteady Wake Characteristics of Rectangular Cylinder

**Prashant Kumar*** **and Shaligram Tiwari**

Department of Mechanical Engineering, Indian Institute of Technology Madras, Chennai-600036, India

*prashant98.nith@gmail.com

**Abstract.** Present study investigates three-dimensional flow field characteristics for flow past surface mounted finite height rectangular cylinder using Open Source Field Operation and Manipulation (OpenFOAM). Wake characteristics have been examined for different values of Reynolds number (Re) ranging from 140 to 200 and fixed height of the cylinder. Different values of side ratio (SR, ratio of longitudinal dimension to transverse dimension of the cylinder) have been considered varying from 0.5 to 3.0 for Re = 180. Effect of Re on unsteady wake flow has been presented using iso $\lambda_2$-surfaces. Unsteady periodic oscillation and effects of Re and SR on wake transition have been illustrated using Hilbert spectra of the transverse velocity signals in the wake. Wake shedding frequency and its distribution in energy frequency domain have been presented and analysed using marginal and Fourier spectra. Comparison between the two spectra reveals that marginal spectra extract lowest frequency which is not captured by Fourier spectra. Extent of nonlinear fluctuations in the wake and its distribution with the associated frequency have been analysed and quantified in terms of degree of stationarity. Variation in mean drag coefficient with change in Re and SR has also been reported.

## 1. Introduction

Surface mounted finite-height cylinders of various cross-sections have been studied extensively over a wide range of Reynolds number (Re) by various researchers both experimentally and numerically due to its practical significance. These applications include flows over buildings, cooling towers and offshore structures, to name a few, at high Re and mini heat exchangers and electronic chips at low Re.

For flow past surface mounted finite height square cylinder, vortex formation, vortex shedding pattern and distribution of dynamic forces depend upon aspect ratio (AR, ratio of height to side length of cylinder), boundary layer thickness and flow Reynolds number (Re). Vortex shedding pattern is different as compared to von Karman vortex shedding (for infinite cylinder) because flow is inherently three-dimensional. A counter-rotating vortex pair is formed due to flow separation near the free end of the cylinder, named as 'tip vortex pair' or 'trailing vortex pair' [1, 2]. Another vortex pair is formed near cylinder plate junction behind the cylinder called 'base vortex pair' [2, 3]. Horseshoe or necklace vortex is formed due to flow separation in upstream of cylinder near the plate surface. Experimental investigations by Kawamura *et al*. [1] of cylinders having slenderness ratio 1 to 8 at Re = 32,000 show that drag coefficient decreases with decrease in height of the cylinder. They have also reported variation in vortex shedding frequency and circumferential pressure distribution for different values of slenderness ratio. Effects of trailing and necklace vortices on variation of wake Strouhal number (St) and lift and drag forces in the spanwise direction have been studied numerically using Lattice Boltzmann method by Liu *et al*. [4] for AR = 10 and Re ranging from 100 to 200. Direct numerical simulation

(DNS) for flow past surface mounted finite height square cylinder shows that flow is steady for AR equal to 2 and unsteady with anti-symmetric mode of vortex shedding for AR ≥ 3 at Re = 250 [5]. DNS computations have been carried out for wall mounted square cylinder of AR = 4 and Re varying from 50 to 1000 by Zhang *et al*. [6]. They observed that formation of mean streamwise vortex structure strongly depends on Re and three different structures are formed depending on ranges of Re, viz. dipole type, quadrupole type and six vortex type. Transitions in the wake from steady to turbulence have been reported by Rastan *et al.* [7] for AR = 7. They reported that unsteadiness triggers in the range of Re from 75 to 85. Wake instability intensifies for Re values between 150 and 200 and finally flow becomes turbulent for Re > 200.

Present study deals with flow past surface mounted rectangular cylinder with varying side ratio (SR, ratio of longitudinal dimension to transverse dimension of the cylinder) for fixed height of the cylinder. Unsteady wake characteristics have been investigated for different values of Re in the range of 140 to 200 for SR = 1.0 and SR varied from 0.5 to 3.0 for Re = 180. Effects of Re and SR on transient fluctuations in the wake have been disclosed using Hilbert spectra and quantified with the help of degree of stationarity.

## 2. Problem formulation

Figure 1 shows schematic of three-dimensional computational domain of finite height square cylinder mounted on a plate surface. Side ratio (SR = $b/d$) is defined as ratio of longitudinal to transverse dimension of the cylinder. Transverse dimension ($d$) is the characteristic dimension and has been kept fixed. Longitudinal dimension ($b$) is varied such that SR = 0.5, 1.0, 1.2, 1.5, 1.8, 2.0, 2.5 and 3.0. Height ($H$) of the cylinder is fixed and is equal to $4d$. Length, width and height of the computational domain are $L_1 = 32d$, $L_2 = 10d$ and $L_3 = 10d$ with origin of the coordinate system fixed at the base of cylinder as shown in figure 1. Cylinder is placed at a distance of $8d$ from inlet. Uniform velocity has been considered at the inlet corresponding to Re values of 140, 160, 180 and 200.

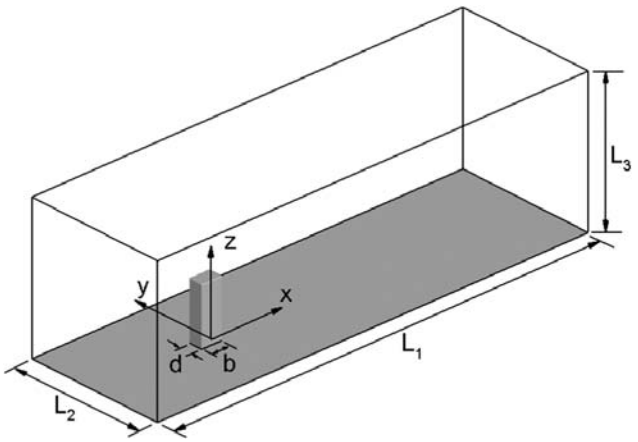


**Figure 1.** Schematic of three-dimensional computational domain.

## 3. Governing equations and boundary conditions

### *3.1. Governing equations*

Three-dimensional unsteady momentum and continuity equations have been solved considering laminar and incompressible flow. Non-dimensionalized form of mass and momentum conservation equations in indicial form can be represented as

$$\frac{\partial u_i}{\partial x_i} = 0 \tag{1}$$

$$\frac{\partial u_i}{\partial t} + \frac{\partial (u_i u_j)}{\partial x_j} = -\frac{\partial p}{\partial x_i} + \frac{1}{\mathrm{Re}}\left(\frac{\partial^2 u_i}{\partial x_j \partial x_j}\right) \tag{2}$$

where $u_i$ and $x_i$ are non-dimensionalized velocity component and spatial coordinate respectively in the $i^{th}$ direction. The velocity components $u_i$ along the *x*, *y* and *z*-directions are *u*, *v* and *w* respectively. Velocity components and coordinate directions are non-dimensionalized using free-stream velocity ( $U_\infty$ ) and size (*d*) of the cylinder respectively. Pressure (*p*) is non-dimensionalized using $\rho U_\infty^2$, where $\rho$ is density of fluid. Reynolds number (Re) based on characteristic velocity ($U_\infty$) and characteristic dimension (*d*) is defined as $\mathrm{Re} = \frac{U_\infty d}{\nu}$, where $\nu$ is kinematic viscosity of the fluid.

*3.2. Boundary conditions*

Boundary conditions prescribed at cylinder and different surfaces of the computational domain are summarized below.

- Inlet: Uniform velocity, ($u = U_\infty$, $v = w = 0$)
- Outlet: Pressure outlet, ( $p = p_\infty$ )
- Cylinder and plate surfaces: No-slip and impermeable boundary conditions, ( $u = v = w = 0$ )
- Top surface: Free-slip and impermeable boundary conditions, $\left( w = 0, \frac{\partial u}{\partial z} = 0, \frac{\partial v}{\partial z} = 0, \frac{\partial p}{\partial z} = 0 \right)$
- Side surfaces: Periodic boundary conditions

## 4. Grid and numerical technique

*4.1. Grid independence study*

Grid mesh has been generated using commercial software ANSYS ICEM CFD 17.2. Structured hexahedral grid with high grid density near cylinder surface has been used as shown in figure 2. Grid independence study has been carried out for both radial and circumferential grid distributions for square cross-section cylinder, i.e. SR = 1.0 at Re = 180. Mean drag coefficient ($Cd_{mean}$) for four different grid divisions around circumference of the cylinder and corresponding total number of nodes has been reported in table 1(a). It can be noted that % change in the value of $Cd_{mean}$ is insignificant as the number of grid divisions changes from 120 to 140. Grid convergence study has been further extended for near wall grid size ($\Delta r$). Four different values of $\Delta r$ and corresponding total number of nodes and $Cd_{mean}$ has been reported in table 1(b). No significant change in the value of $Cd_{mean}$ has been witnessed as the values of $\Delta r$ reduce from 0.007 to 0.005. Accordingly, all the computations have been performed considering 0.007 as near wall grid size with 120 grid divisions around circumference of the cylinder.

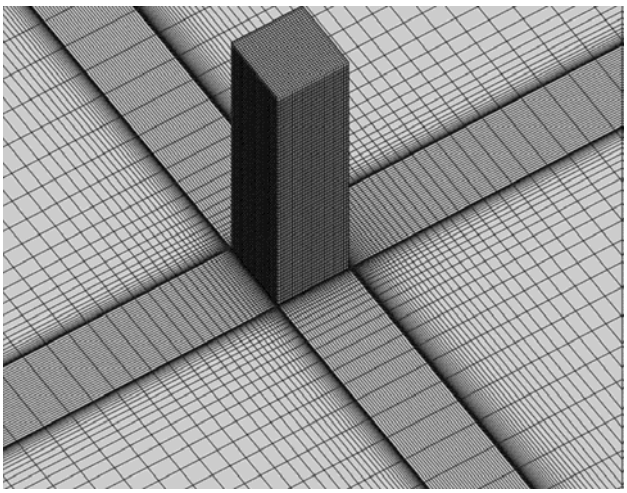

**Figure 2.** Grid distribution around the cylinder.

**Table 1(a).** Mean drag coefficient ($Cd_{mean}$) for different grid divisions around the cylinder.

| Grid | Grid divisions around the cylinder | Total no of nodes | $Cd_{mean}$ | % change |
|---|---|---|---|---|
| G1 | 80 | 822780 | 1.2216 | 0.573 |
| G2 | 100 | 992210 | 1.2286 | 0.187 |
| **G3** | **120** | **1130750** | **1.2309** | **0.065** |
| G4 | 140 | 1310620 | 1.2317 | - |

**Table 1(b).** Mean drag coefficient ($Cd_{mean}$) for different values of near wall grid size.

| Grid | Near wall cell size | Total no of nodes | $Cd_{mean}$ | % change |
|---|---|---|---|---|
| G1 | 0.013 | 829160 | 1.2207 | 0.696 |
| G2 | 0.010 | 982370 | 1.2292 | 0.219 |
| **G3** | **0.007** | **1127380** | **1.2319** | **0.057** |
| G4 | 0.005 | 1321230 | 1.2326 | - |

*4.2. Numerical technique*

Governing equations have been solved using Open Source Field Operation and Manipulation (OpenFOAM) C++ libraries based on finite volume discretization on collocated grids. Pressure and velocity coupling have been resolved using Pressure Implicit with Splitting of Operators (PISO) algorithm with two PISO corrector loops. Convective term is discretized using Gauss cubic scheme. Pressure and diffusive terms are discretized using Gauss linear scheme. First order Euler implicit scheme is employed for time marching in the momentum equation. For accuracy and numerical stability of time derivative, time step has been adopted such that maximum Courant number remains below 0.5 for all the computations. For pressure and momentum convergence in every time step, absolute convergence criteria is set as $10^{-6}$.

## 5. Results and discussion

*5.1. Validation of computations*

Numerical scheme used in present computations has been validated with direct numerical simulations (DNS) for flow past finite height square cylinder (AR = 3) mounted on a plate surface at Re = 250. Variation of time-averaged streamwise velocity component ($u_{mean}$) along transverse direction ($y$-direction) has been plotted from the present computations at $x$ = 3 and $z$ = 2.5 and compared with variation reported by Saha [5]. Streamwise velocity distribution is found to be similar to the variation observed using DNS [5].

*5.2. Three-dimensional instantaneous flow structure*

Vortical motion in the wake has been identified and presented using $\lambda_2$-criteria and defined as second largest eigen value of the tensor, $S^2 + \Omega^2$, where $S$ is strain rate tensor and $\Omega$ is vorticity tensor [8]. For visualizing sense of rotation of vortices, z-vorticity is superimposed on iso $\lambda_2$-surfaces of magnitude 0.02. Red and blue contours show anti-clockwise and clockwise sense of rotation respectively.

Figure 4 shows iso $\lambda_2$-surfaces for SR = 1.0 and different values of Re. Flow is found to be unsteady with anti-symmetric mode of vortex shedding for all values of Re. For Re = 140, long streamwise slender structures are formed and detach alternatively from side surfaces of the cylinder as shown in figure 4(a). However, with increase in Re, hairpin vortices are observed in the wake region. Furthermore, the wake seems more disorganized as these vortices shed early (length of shear layer decreases) with increase in Re. Figure 5 shows iso $\lambda_2$-surfaces for different values of SR at Re = 180. Flow is observed to be unsteady with formation of hairpin vortices up to SR = 1.5. For higher values of SR ($\geq$ 1.8), time independent flow has been observed with formation of long streamwise slender structures as shown in figures 5(e) and (f).

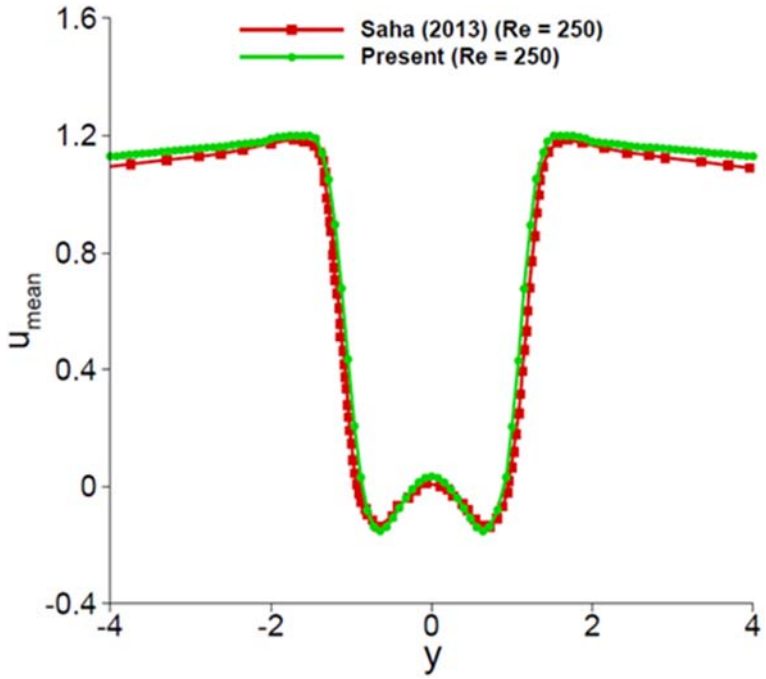


**Figure 3.** Variation of $u_{mean}$ along transverse direction ($y$-direction) for AR = 3 at $x$ = 3 and $z$ = 2.5.

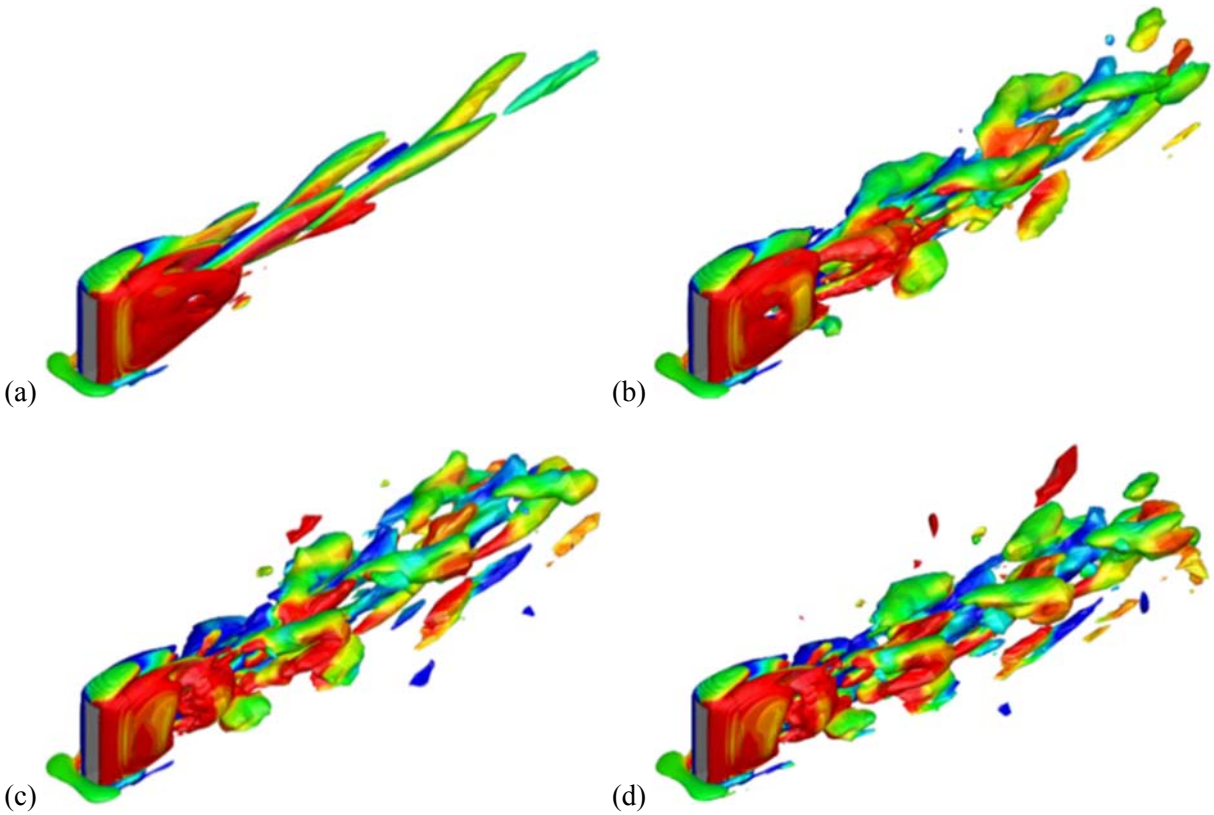


**Figure 4.** Instantaneous iso $\lambda_2$-surfaces, colored with z-vorticity, for SR = 1.0 and different values of Re (a) Re = 140 (b) Re = 160 (c) Re = 180 (d) Re = 200.

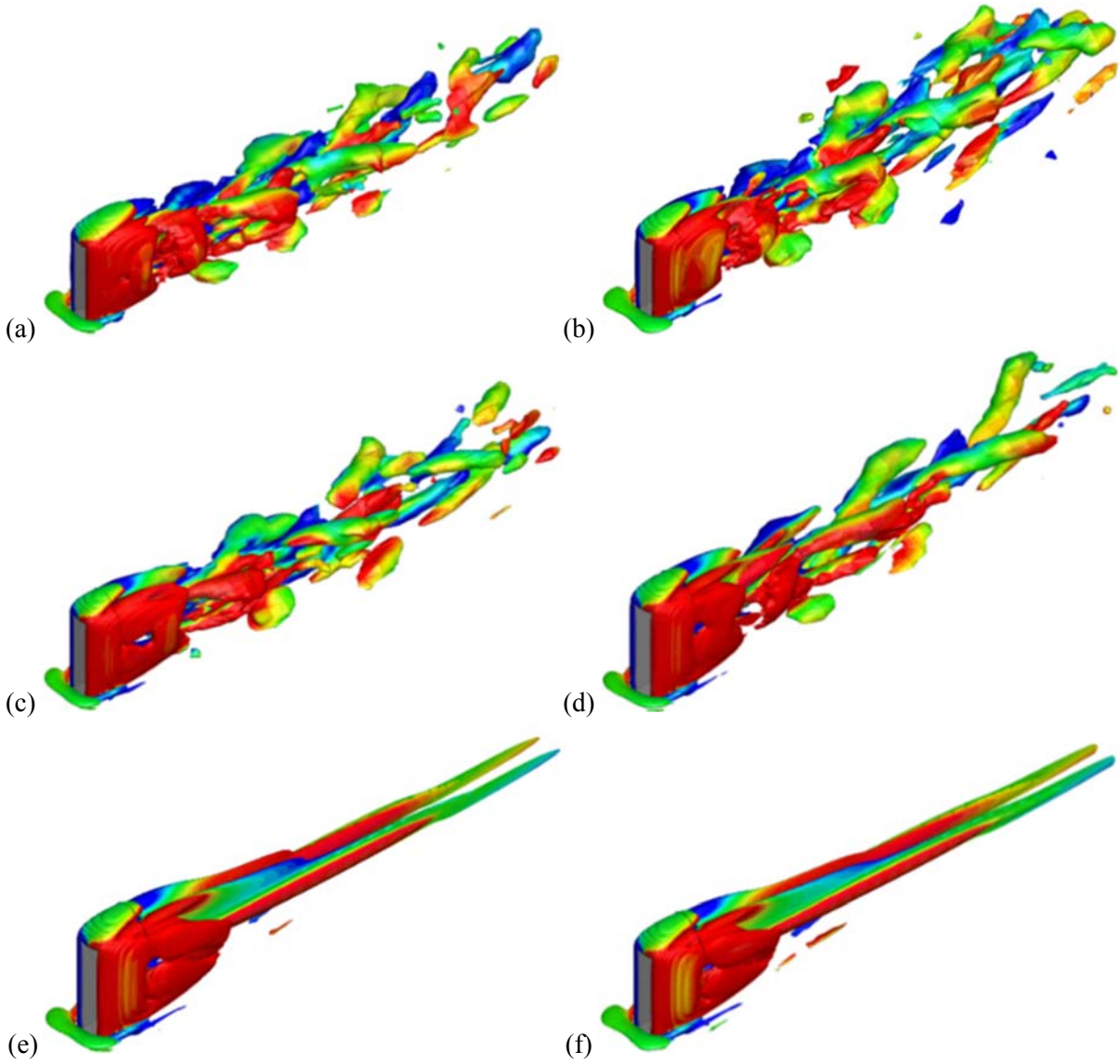


**Figure 5.** Instantaneous iso $\lambda_2$-surfaces, colored with z-vorticity, for Re = 180 and different values of SR (a) SR = 0.5 (b) SR = 1.0 (c) SR = 1.2 (d) SR = 1.5 (e) SR = 1.8 (f) SR = 2.0.

*5.3. Hilbert Huang transformation (HHT)*

Fast Fourier transform (FFT) is a powerful toll for decomposition of linear systems and stationary or periodic data over time into basis functions of constant amplitude and frequency. Deviation from stationarity of the time series data indicates multiple spurious harmonics that result in spreading of energy revealing less physical meaning [9]. HHT offers decomposition of any multi-component complex signal into different mono-component basis functions without loss of physical and realistic information as basis functions are obtained from the primary signal. Frequency of component signals, named as "instantaneous frequency (IF)", varies locally with time. The primary outcome of HHT is frequency-energy-time distribution of each decomposed signal known as "Hilbert spectra". Different operations involved in HHT have been explained in Neeraj and Tiwari [10].

Transverse velocity components for different values of Re and SR have been depicted in figures 6(a) and 6(b) respectively. Amplitude of velocity signals increases with increase in Re while it decreases with increase in SR. Hilbert spectra corresponding to transverse velocity signals for SR = 1.0 and different values of Re have been illustrated in figure 7. Variation of IF with time is labelled on y-axis in the Hilbert spectrum. Contours show square of amplitude or energy density corresponding to each IMF

in the Hilbert spectra. Red and blue colours in the contour represent maximum and minimum energy density. Appearance of different waveforms in the spectra represents IF distribution corresponding to IMFs. For an IMF similar to harmonic function (sine or cosine) frequency is constant over time indicates straight line in the spectra. Increase in bandwidth of IMF indicates intra-wave modulations showing deviation from harmonic function. On the other hand, intermixing of IMFs indicates inter-wave modulations. Existence of inter-wave and intra-wave modulations is a signature of nonlinear fluctuations in the wake. Presence of different distinguishable frequency bands in the Hilbert spectra reveals strong periodic flow behaviour while intermixing of IMFs indicates aperiodic flow behaviour signifying strong nonlinearity.

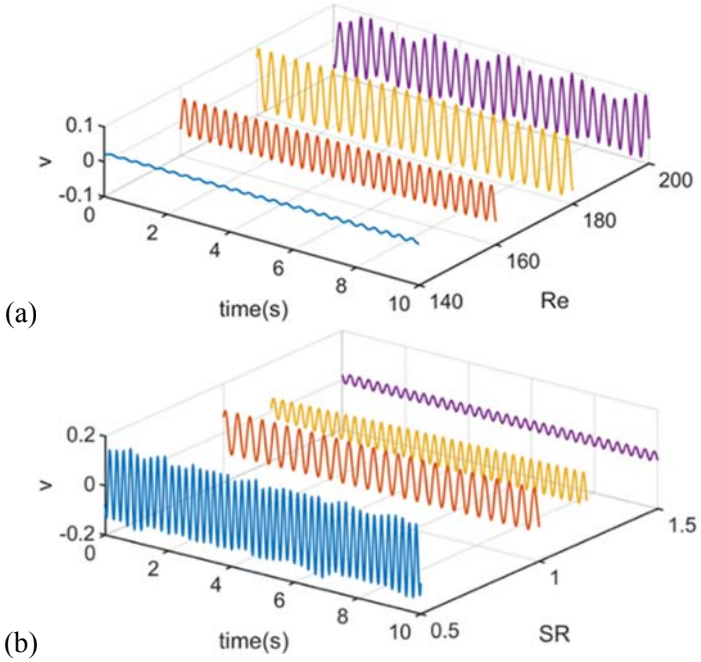


**Figure 6.** Time signals of transverse velocity component for different values of (a) Re and (b) SR.

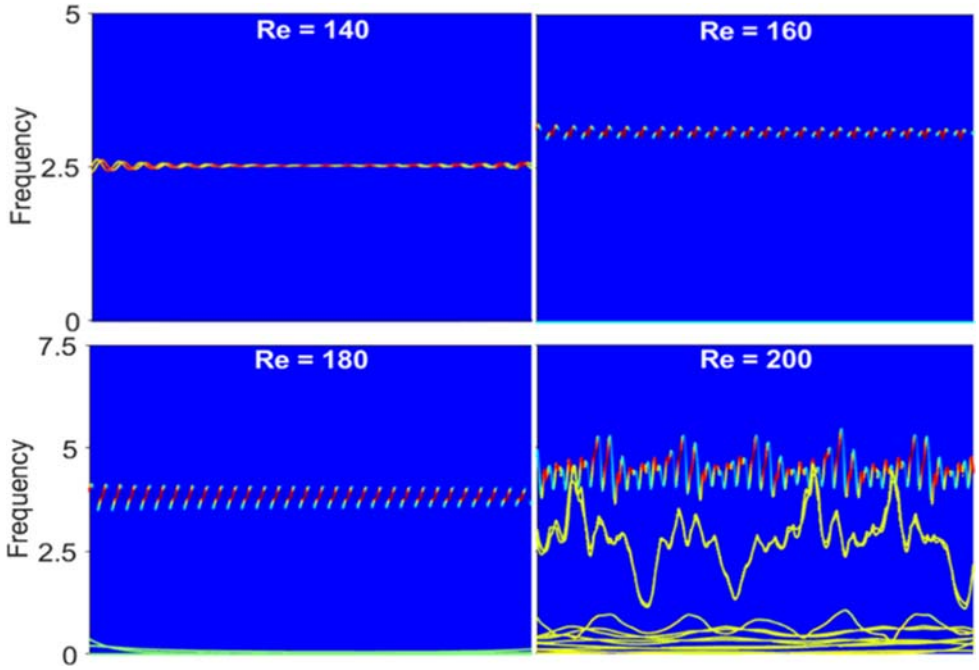


**Figure 7.** Hilbert spectra of transverse velocity signals for SR = 1.0 and different values of Re.

For Re = 140, 160 and 180, appearance of IMFs in different frequency bands is an indication of strong periodic flow. However, at Re = 200, inter-wave and intra-wave modulations indicate that nonlinearity intensifies and the wake oscillations do not remain periodic. Furthermore, with increase in Re, mean frequency and bandwidth of the dominant frequency increases, signifying increase in nonlinear fluctuations as shown in figure 7. Effect of SR on frequency distribution at Re = 180 is shown in figure 8. Flow is observed to be periodic for all values of SR except for SR = 0.5. Presence of low frequency IMFs in the Hilbert spectrum for SR = 0.5 disturbs the periodicity of the wake. It is interesting to note that with increase in SR, wake stabilizes as indicated by decease in intra-wave frequency modulations and decrease in mean dominant frequency.

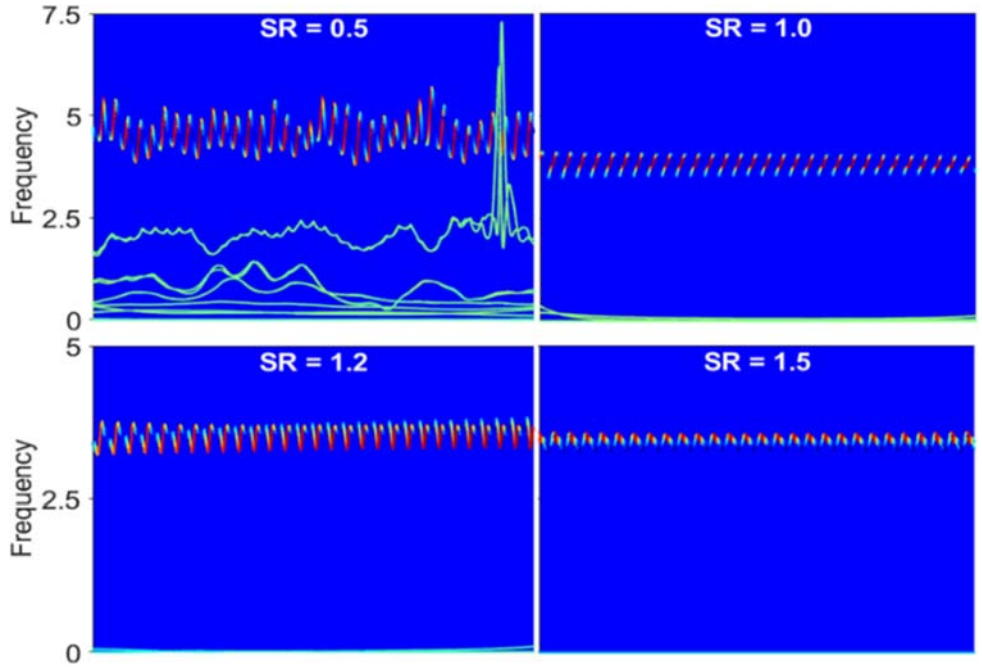


**Figure 8.** Hilbert spectra of transverse velocity signals for Re = 180 and different values of SR.

Frequency-energy distribution extracted from the Hilbert spectra has been represented in marginal spectra. Figure 9 shows marginal spectra (left) and Fourier spectra (right) for different values of Re and SR. HHT is distinguished from other standard techniques due to its capability of decomposition of a signal into lowest possible frequency of the component signals. For Re = 180 and 200, different spikes can be witnessed in the marginal spectrum in the frequency range of 2.5 to 4.8 Hz. On the other hand, only single frequency appears in the Fourier spectrum. In addition, very low frequency components can be observed in the marginal spectrum which disturbs the periodicity of the wake. Similarly, for, SR = 0.5, multiple peaks are present in the marginal spectrum over wide range of frequencies indicating strong nonlinear wake oscillations as shown in figure 9(b). However, single dominant peak appears in the Fourier spectrum indicating wake is periodic with this frequency. The upper edge of HHT over other techniques is that it quantifies the nonlinear fluctuations present in a time signal. An index that provides such variation with frequency is expressed in terms of 'degree of stationarity DS(f)'. Figure 10 illustrates distribution of DS(f) with frequency for different values of Re and SR. It can be observed that value of DS(f) intensifies over range of frequencies with increase in Re and is found to be maximum at Re = 200 indicating maximum nonlinear interactions in the wake. However, for lower values of Re (= 140 and 160), appearance of single peak signifies nonlinearity is involved only with the dominant frequency as shown in figure 10(a). Extent of nonlinear fluctuation is witnessed to be maximum for SR = 0.5 and decreases with increase in SR as shown in figure 10(b).

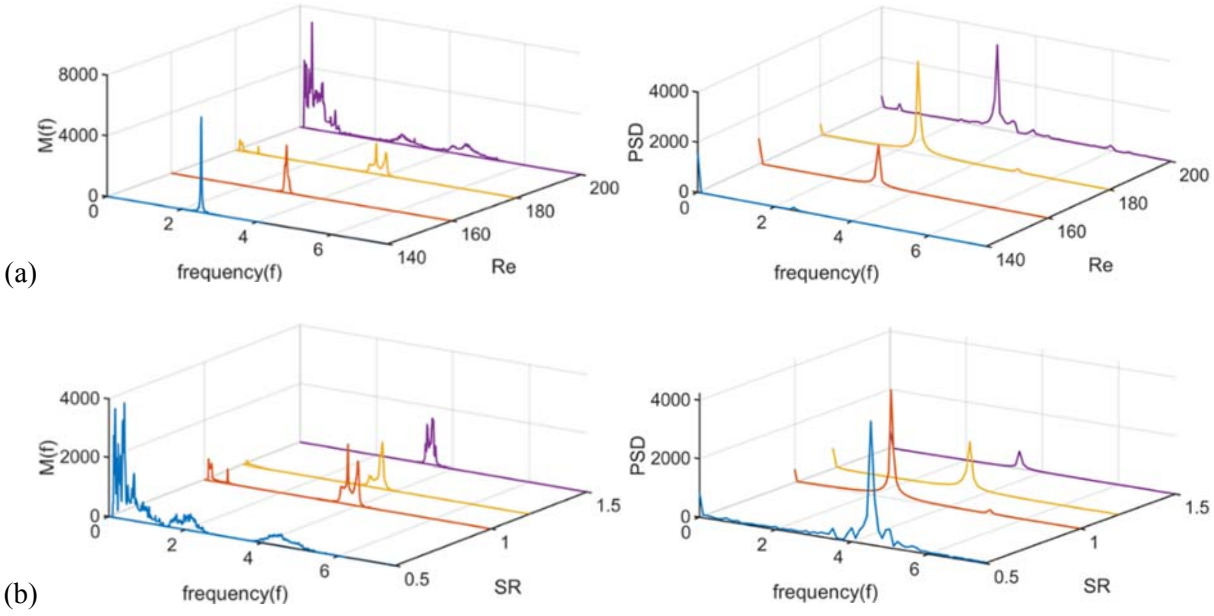


**Figure 9.** Marginal spectra (left) and Fourier spectra (right) for different values of (a) Re (b) SR.

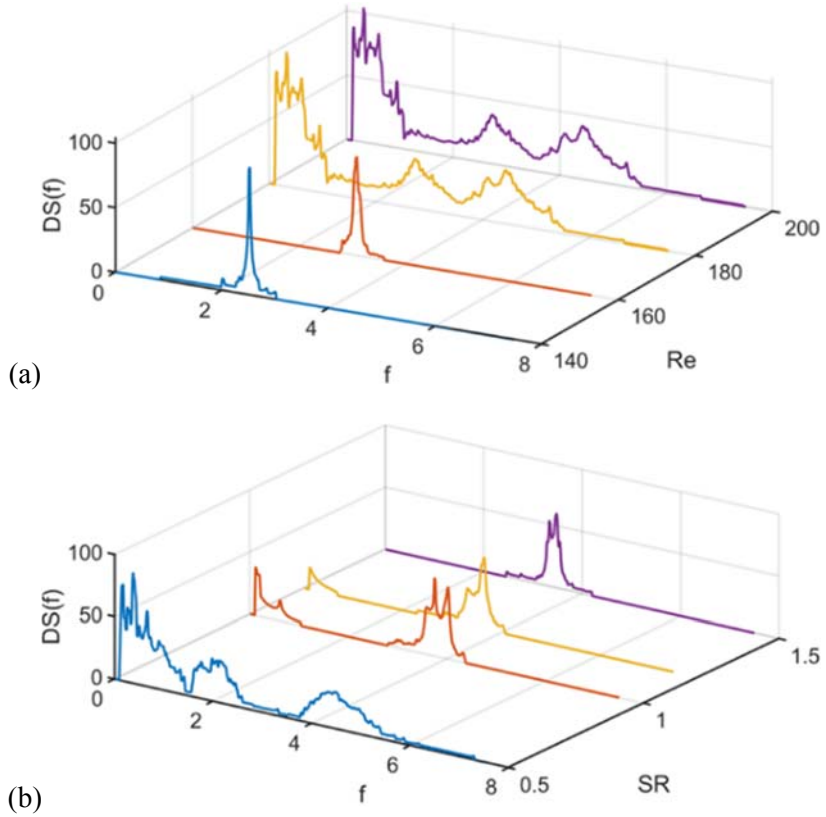


**Figure 10.** Degree of stationarity for different values of (a) Re (b) SR.

*5.4. Dynamic characteristic*

Figures 11(a) and 11(b) show variation in mean drag coefficient ($Cd_{mean}$) with change in Re and SR respectively. $Cd_{mean}$ is found to increase with increase in Re and is maximum at Re = 200 for SR = 1.0. On the other hand, it decreases with increase in SR of the cylinder at Re = 180 as shown in figure 11(b). For SR = 0.5, large recirculation region behind the cylinder causes more pressure drop resulting in maximum drag force on the cylinder.

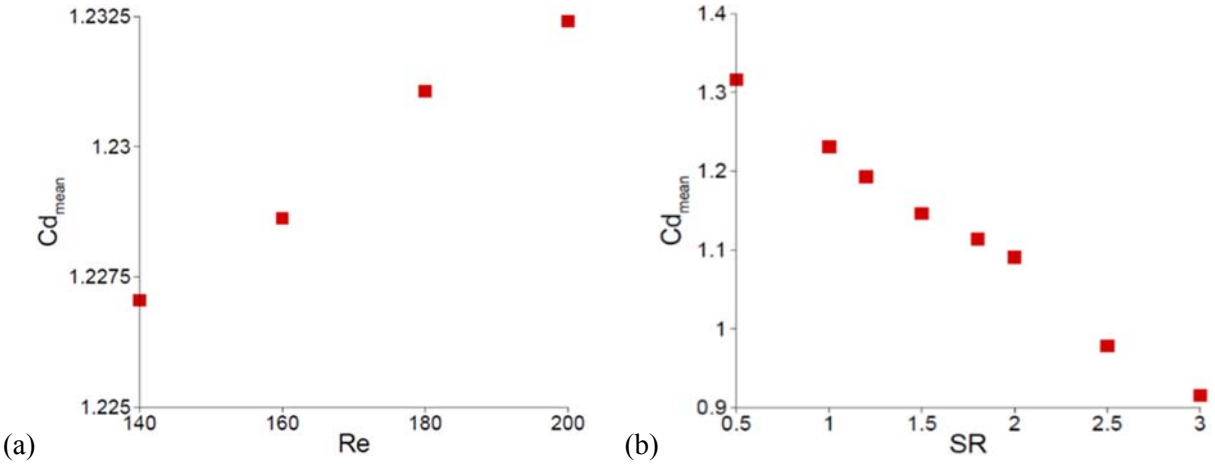


**Figure 11.** Variation of $Cd_{mean}$ for different values of (a) Re (b) SR.

## 6. Conclusions

Three-dimensional unsteady flow characteristics have been examined using Hilbert Huang transformation of time series signals in the wake. Flow is observed to be time dependent at all values of Re ranging from 140 to 200 for SR = 1.0. On the other hand, flow is found to be steady for SR ≥ 1.8 at Re = 180 with formation of long streamwise vortices. With increase in Re, intra-wave modulations of the waveform increase and attain maximum at Re = 200 for SR = 1.0, while modulations decrease with increase in SR and achieve minimum for SR = 1.5 at Re = 180. Flow is found to be aperiodic at Re values of 180 and 200 for SR = 0.5 and 1.0 respectively as different peaks appear in the marginal spectra. Mean drag coefficient is found to increase with increase in Re and decrease with increase in SR.

## References

[1] Kawamura T, Hiwada M, Hibino T, Mabuchi T and Kumada M 1984 Flow around a finite circular cylinder on a flat plate *Bull. JSME* **27** 2142-2151.
[2] Sumner D, Heseltine J L and Dansereau O J P 2004 Wake structure of a finite circular cylinder of small aspect ratio *Exp. Fluids* **37** 720-730.
[3] Tanaka S and Murata S 1999 An investigation of the wake structure and aerodynamic characteristics of a finite circular cylinder *JSME Int. J., Series B: Fluids Thermal Engineering* **42** 178-187.
[4] Liu Y, So R M C and Cui Z X 2005 A finite cantilevered cylinder in a cross-flow *J. Fluids Struct.* **20** 589-609.
[5] Saha A K 2013 Unsteady flow past a finite square cylinder mounted on a wall at low Reynolds number *Comput. & Fluids* **88** 599-615.
[6] Zhang D, Cheng L, An H and Zhao M 2017 Direct numerical simulation of flow around a surface-mounted finite square cylinder at low Reynolds numbers *Phys. Fluids* **29** 045101.
[7] Rastan M R, Sohankar A and Alam Md. M 2017 Low-Reynolds-number flow around a wall-mounted square cylinder: Flow structures and onset of vortex shedding *Phys. Fluids* **29** 103601.
[8] Jeong J and Hussain F 1995 On the identification of a vortex *J. Fluid Mech.* **285** 69-94.
[9] Huang N E, Shen Z, Long S R, Wu M C, Shih H H, Zheng Q, Yen N C, Tung C C and Liu H H 1998 The empirical mode decomposition and the Hilbert spectrum for nonlinear and non-stationary time series analysis *Proceedings of the Royal Society of London A: Mathematical, Physical and Engineering Sciences* **454** 903-995.
[10] Neeraj M P and Tiwari S 2019 On wake analysis of flow past rotating downstream cylinder using Hilbert-Huang transformation *J. Applied Fluid Mech.* **12** 175-186.